Influence of limited-view scanning on depth imaging of photoacoustic tomography*

Wu Dan(吴 丹)[a], Tao Chao(陶 超)[a]†,
Liu Xiao-Jun(刘晓峻)[a]‡, and Wang Xue-Ding(王学鼎)[b]

[a] *Key Laboratory of Modern Acoustics of Ministry of Education, Nanjing University, Nanjing* 210093, *China*
[b] *Department of Radiology, University of Michigan, Ann Arbor, Michigan* 48109, *USA*

(Received 14 June 2011; revised manuscript received 27 July 2011)

We study the influence of limited-view scanning on the depth imaging of photoacoustic tomography. The situation, in which absorbers are located at different depths with respect to the limited-view scanning trajectory, is called depth imaging and is investigated in this paper. The results show that limited-view scanning causes the reconstructed intensity of deep absorbers to be weaker than that of shallow ones and that deep absorbers will be invisible if the scanning range is too small. The concept of effective scanning angle is proposed to analyse that phenomenon. We find that an effective scanning angle can well predict the relationship between scanning angle and the intensity ratio of absorbers. In addition, limited-view scanning is employed to improve image quality.

Keywords: photoacoustic tomography, limited-view scanning, depth imaging, back-projection reconstruction

PACS: 43.35.Ud, 43.20.Ks, 43.60.Pt **DOI:** 10.1088/1674-1056/21/1/014301

1. Introduction

Photoacoustic tomography (PAT)[1−7] is a novel imaging modality based on the photoacoustic effect. In biomedical PAT, after irradiation by a non-ionizing pulsed laser, biological tissues absorb optical energy, and convert it into heat. The heat eventually leads to transient thermoelastic expansion and wideband (e.g. MHz) ultrasonic emission. This is the so-called photoacoustic effect.[8,9] The generated ultrasound is then detected by an ultrasonic transducer. From the detected photoacoustic signals, the optical absorption deposition inside tissues is finally reconstructed to form an image.

PAT combines the advantages of both ultrasonic and optical methods available in medical imaging. Firstly, PAT can provide better contrast than ultrasonic imaging, because the primary contrast in PAT is optical absorption, instead of acoustic impedance. PAT is significantly effective for imaging physiological properties which are closely associated with optical absorption, such as hemoglobin concentration and oxygen saturation. Secondly, PAT can overcome the overwhelming scattering of light in biological tissues. Since the scattering intensity of ultrasound is 2–3 orders of magnitude weaker than that of optical waves, PAT can provide higher spatial resolution for deep biological tissues (> 1.0 mm in depth) than optical imaging. Thirdly, unlike ionizing X-ray radiation, the non-ionizing wave used in PAT poses no health hazards. Due to the advantages mentioned above, PAT has aroused broad interest and has already been widely applied in biomedical imaging, such as simultaneous transcranial imaging of oxygen saturation and concentration of hemoglobin,[10] photoacoustic angiography of the brains of rats *in vivo*,[11] and structural tomography of the joints of animals and humans.[12−14]

Many previous studies on PAT concentrated on full-view tomography,[15−17] which denotes that the image is reconstructed from the whole photoacoustic signals surrounding the region of interest. In other words, the image is reconstructed from the signals collected on a closed circle for two-dimensional cases or on a closed sphere for three-dimensional cases. Unfortunately, in practice, due to the scattering or reflec-

*Project supported by the National Basic Research Program of China (Grant No. 2012CB921504), the National Natural Science Foundation of China (Grant Nos. 10874088, 10904069, and 11028408), and the Natural Science Foundation of Jiangsu Province, China (Grant No. SBK201021985).

†Corresponding author. E-mail: taochao@nju.edu.cn
‡Corresponding author. E-mail: liuxiaojun@nju.edu.cn

© 2012 Chinese Physical Society and IOP Publishing Ltd

tion of the complex structures in tissues, photoacoustic signals cannot always be completely collected from all orientations. For example, the solid angle of detection for breasts is at most 2π in a hemisphere form. Therefore, one has to face the problem of limited-view tomography during the application of PAT. Due to its practical importance, a great deal of attention has been paid to obtain PAT from incomplete photoacoustic data.[18−21] It has been found that for two separated absorbers situated on a line parallel to the scanning trajectory, incomplete data could make them indiscriminate in the reconstructed image, thus degrading resolution.[18]

For full-view PAT, the photoacoustic signals are collected on a closed curve or surface. The problem that some areas are closer to the scanning trajectory than other areas does not exist. However, for limited-view PAT, the scanning trajectory is only a short arch or line. As shown in Fig. 1, the solid arch denotes limited-view scanning trajectory, and the two solid circles denoted as S_N and S_F represent absorbers. In this case, the absorber S_N is closer to the trajectory than the absorber S_F. Therefore, limited-view scanning results in the fact that the absorbers could be situated at different depths with respect to the scanning trajectory. This scenario is named depth imaging of PAT in this study. To the best of our knowledge, until now, the influence of limited-view scanning on depth imaging has not been carefully examined in previous works.

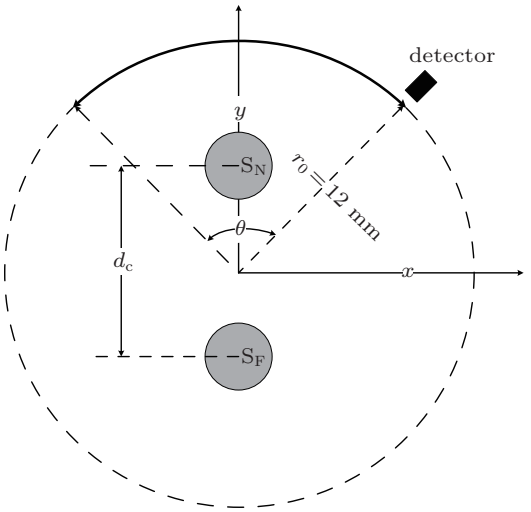


Fig. 1. Schematic diagram of the numerical experiment setup, where d_c is the distance between the centers of the absorbers.

In this study, numerical experiments based on the finite element method (FEM) are used to simulate the generation, propagation, and reception of the photoacoustic signals. The back-projection algorithm, which has been widely applied in PAT, is used to reconstruct the image from incomplete photoacoustic data. The tomographies of absorbers located at different depths are studied. This paper is organized as follows: in Section 2, the setup of numerical experiments is introduced and the back-projection reconstruction algorithm is briefly reviewed. In Section 3, numerical experiments based on FEM are implemented to investigate the influence of limited-view scanning on depth imaging of PAT. Finally, the conclusion is drawn in Section 4.

2. Methods

2.1. Numerical experimental setup

The setup of the numerical experiments is shown in Fig. 1. A pair of optical absorbers are surrounded by a non-absorbing and homogenous background medium. The two small solid circles represent the absorbers. The centers of the absorbers (S_N and S_F) are located on the y axis, and they are symmetrical with respect to the x axis. The absorbers are 1.0 mm in radius. The medium and the absorbers are assumed to have the same sound speed ($c = 1500$ km/s) and density ($\rho = 1000$ kg/m^3). The relative absorption intensity $A(\boldsymbol{r})$ of absorbers is 1.0, while $A(\boldsymbol{r})$ of the medium is 0.0. A Gaussian pulse with central frequency of 2 MHz is used to simulate the initial pressure generated by the photoacoustic effect. The photoacoustic wave is detected by a small-size transducer scanning along a circle (the big circle in Fig. 1), with radius $r_0 = 12$ mm. The solid arch in Fig. 1 represents the actual limited-view scanning trajectory. The trajectory is designated to be symmetrical with respect to the y axis. The generation, propagation, and reception of the photoacoustic signals are simulated with the acoustics module in software COMSOL 3.5.

The scanning angle θ, as shown in Fig. 1, is used to quantify the angular range of the limited-view scanning. Apparently, $\theta = 2\pi$ denotes the full-view scanning case, whereas $\theta < 2\pi$ represents the limited-view case.

2.2. The back-projection reconstruction algorithm

The back-projection reconstruction algorithm was used to reconstruct the relative absorption intensity distribution $A(\boldsymbol{r})$. If the laser pulse is extremely narrow so that it can be approximate to a Dirac delta function $\delta(t)$ and the detection of photoacoustic wave satisfies the far-field condition $kr_0 \gg 1$ (k is the wave number and r_0 is the detection radius), $A(\boldsymbol{r})$ can be reconstructed using the following equation:

$$A(\boldsymbol{r}) = -\frac{r_0^2}{2\pi\beta c^4} \iint \mathrm{d}\,\Omega_0 \frac{1}{t} \frac{\partial p\,(\boldsymbol{r}_0, t)}{\partial t}\bigg|_{t=|\boldsymbol{r}-\boldsymbol{r}_0|/c}, \quad (1)$$

where c is the speed of sound, β is the isobaric volume expansion coefficient and $p(\boldsymbol{r}_0, t)$ represents the photoacoustic pressure recorded at spatial position $\boldsymbol{r}_0$ and time t. For a two-dimensional circular scanning, Eq. (1) can be simplified to

$$A(\boldsymbol{r}) = -\frac{r_0^2}{2\pi\beta c^4} \oint \mathrm{d}\theta_0 \frac{1}{t} \frac{\partial p\,(\boldsymbol{r}_0, t)}{\partial t}\bigg|_{t=|\boldsymbol{r}-\boldsymbol{r}_0|/c}. \quad (2)$$

In the limited-view case, the ultrasonic transducer cannot detect all the photoacoustic signals on a closed curve or surface, so $A(\boldsymbol{r})$ cannot be directly obtained from Eqs. (1) and (2) through an integral over a whole sphere or circle. By assuming the data on unmeasured view to be zero, the algorithm for full-view data can be approximately extended to the limited-view case. For the two-dimensional limited-view case, $A(\boldsymbol{r})$ can be approximated by

$$A(\boldsymbol{r}) \approx -\frac{r_0^2}{2\pi\beta c^4} \int_{\theta_1}^{\theta_2} \mathrm{d}\theta_0 \frac{1}{t} \frac{\partial p\,(\boldsymbol{r}_0, t)}{\partial t}\bigg|_{t=|\boldsymbol{r}-\boldsymbol{r}_0|/c}. \quad (3)$$

The term $\partial p(\boldsymbol{r}_0, t)/\partial t$ in Eqs. (2) and (3) were calculated through the Fourier transformation as

$$\partial p(\boldsymbol{r}_0, t)/\partial t = \mathrm{IFFT}\left(\mathrm{i}\,\omega p\,(\boldsymbol{r}_0, \omega)\, W\,(\omega)\right), \quad (4)$$

where ω is the angular frequency, $p(\boldsymbol{r}_0, \omega)$ is the Fourier transformation of $p(\boldsymbol{r}_0, t)$, and IFFT denotes the inverse Fourier transformation; $W(\omega)$ is a Hanning window function with an angular cutoff frequency ω_c as

$$\mathrm{W}\,(\omega) = \begin{cases} 0.5 + 0.5\cos\left(\pi\dfrac{\omega}{\omega_\mathrm{c}}\right) & |\omega| \le \omega_\mathrm{c}, \\ 0 & \text{else.} \end{cases} \quad (5)$$

The low-pass window function above simulates the effect of the limited band of the realistic transducer. The cutoff frequency $f_\mathrm{c} = \omega_\mathrm{c}/2\pi$ is 2.5 MHz.

From Eqs. (2) and (3), we can see that the limited-view PAT with a larger scanning angle gives a better approximation of full-view PAT than that with a smaller angle. However, it is yet unknown how the scanning angle influences the quality of reconstruction. That is right what will be discussed in the next section.

3. Results and discussion

FEM was used to simulate the generation and propagation of the photoacoustic signals in biomedical tissues. Numerical experiments based on FEM allow researchers to precisely manipulate the experimental setup, making it easy to study the quantitative relationship between the scanning range and the image quality and giving us a better insight into the physical process of limited-view PAT.

Figure 2 shows the depth imaging with different scanning angles, where the radii of absorbers are $r_\mathrm{s} = 1.0$ mm and the distance between their centers is $d_\mathrm{c} = 6.0$ mm. Panel (a) presents the reconstructed images with $\theta = 2\pi$ (i.e. full-view PAT). In panel (b), the scanning angle is $\theta = \pi$. The incomplete data lead to the distortion of the absorbers in the reconstructed image. Moreover, the shallow absorber $\mathrm{S_N}$ is shown to have stronger reconstructed intensity than the deep absorber $\mathrm{S_F}$. The size of $\mathrm{S_F}$ appears to be smaller than that of $\mathrm{S_N}$. When θ is decreased to 0.5π, the distortion becomes more severe. $\mathrm{S_N}$ becomes larger in size, and $\mathrm{S_F}$ becomes smaller. The difference between $\mathrm{S_N}$ and $\mathrm{S_F}$ is increased. When $\theta = 0.25\pi$, $\mathrm{S_N}$ continues to be stretched and becomes bigger. The intensity of $\mathrm{S_F}$ is smaller than the half-maximum value of $\mathrm{S_N}$; therefore, it looks like that $\mathrm{S_F}$ has disappeared in the reconstructed image.

The above results show that a deep absorber can have such a weak reconstructed intensity that it is obscured by the shallow absorber, which is likely to cause the disappearance of $\mathrm{S_F}$, even if they are actually the same in the original optical absorption property. The disappearance of the deep absorber is called depth invisibility in this study. Note that acoustic and optical attenuations are both ignored in this simulation. Limited-view scanning is the only reason for depth invisibility.

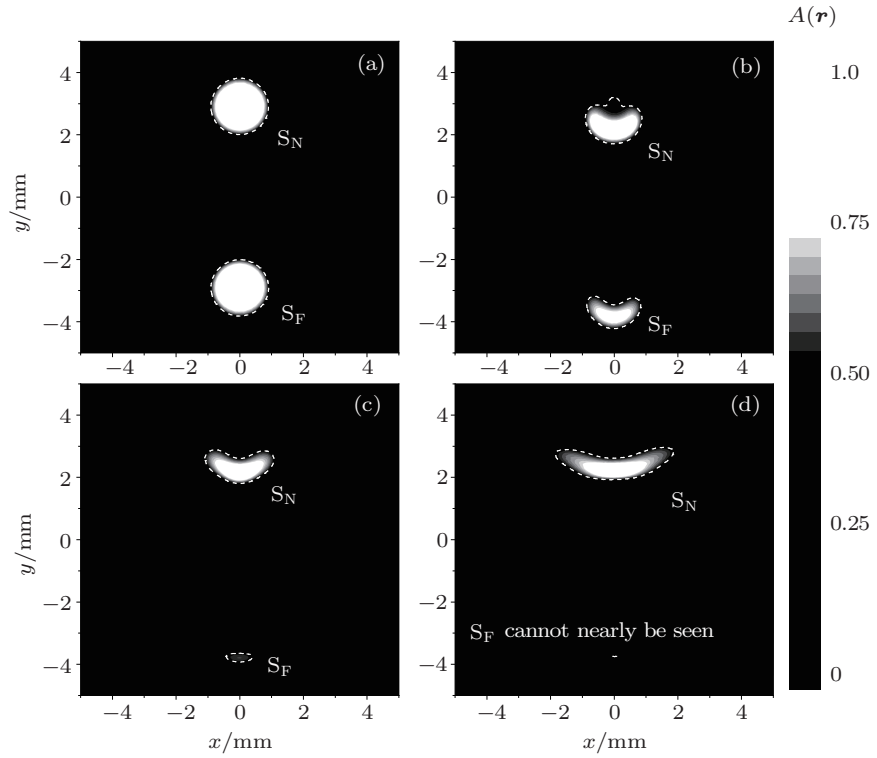


Fig. 2. Depth imaging with different scanning angles: (a) $\theta = 2\pi$, (b) $\theta = \pi$, (c) $\theta = 0.5\pi$, (d) $\theta = 0.25\pi$. The dashed lines are the half-maximum contour lines.

To explain the phenomenon induced by limited-view scanning and obtain a better understanding of the above-mentioned numerical simulation, limited-view imaging of the absorbers at different depths is theoretically analysed in Fig. 3. P_N and P_F represent two point absorbers. Apparently, they are located at different depths. The solid arch is the scanning orbit and θ is the scanning angle. In Fig. 3, effective scanning angle θ_e is defined (θ_N for shallow absorber and θ_F for deep absorber, respectively). Though the scanning angle is the same for both of them, they have different effective scanning angles, because of their different depths. Since P_N is shallower than P_F, P_N has larger effective scanning angle than P_F. The detector could collect about $\theta_F/2\pi \times 100\%$ signals generated by P_F, but $\theta_N/2\pi \times 100\%$ signals by P_N. Even if the same amount of energy is given out from P_F and P_N , the actual energy received by the detector could be different due to their different effective scanning angles. Therefore, the absorbers which have the same absorption coefficient but are located at different depths have different reconstructed intensities. Based on the above analysis, the reconstructed intensity ratio between P_F and P_N can be approximated by the following equation:

$$\eta\,(d_F, d_N, \theta) = \frac{\alpha_F \theta_F(d_F, \theta)}{\alpha_N \theta_N(d_N, \theta)}, \qquad (6)$$

where α_N and α_F represent the absorption coefficients of P_N and P_F, θ_N and θ_F are the effective scanning angles of P_N and P_F, d_N and d_F are the depths of P_N and P_F, respectively, and θ is the scanning angle. Obviously, the effective scanning angle can be calculated according to the geometric relationship between the scanning angle and the depth of the absorbers, as shown in Fig. 3. The effective scanning angle is a function of scanning angle and depth.

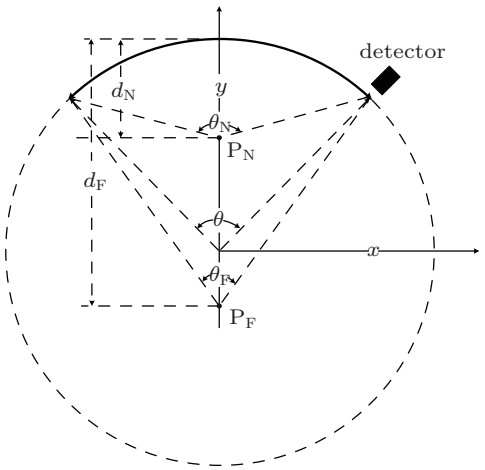


Fig. 3. Analysis of depth imaging, where P_N and P_F are a pair of point absorbers situated at different depths, and d_N and d_F are the depths relative to the scanning surface.

For a full-view scanning case ($\theta = 2\pi$), it has

$\theta_N = \theta_F = 2\pi$. The ratio of the reconstructed intensity of P_N to that of P_F just depends on the ratio of their original absorption coefficients and not on their depths. However, for a limited-view case, θ_N is always greater that θ_F, and a small scanning angle leads to a large ratio θ_F/θ_N. Therefore, even though P_N and P_F have the same absorption coefficient, the reconstructed intensity of P_N turns out to be stronger than that of P_F.

The predictions with Eq. (6) are compared with the results of the numerical experiments. Figure 4(a) gives the maximum intensity ratio η between the absorbers as a function of the scanning angle, where $d_c = 6.0$ mm and $r_s = 1.0$ mm. In general, the ratio η increases with the scanning angle θ. As θ approaches 2π, η approaches the actual amplitude ratio 1.0. Figure 4(b) gives the relationship between η and d_c, where θ is fixed to be 0.5π and the d_c value is changed by moving S_F and S_N symmetrically toward the origin or away from the origin along the y axis. It shows that the maximum intensity ratio declines with the increase of d_c and that the deeper absorber will disappear ($\eta < 0.5$) from the reconstructed image when $d_c > 7.0$ mm. The predictions from Eq. (6) are also plotted in Fig. 4. The ratio between the effective scanning angles of the centers of the absorbers is used to approximate to their maximum intensity ratio. The predictions agree with the numerical results. It is shown that the concept of effective scanning angle can accurately explain the influence of limited-view scanning on depth imaging.

In addition, Fig. 4(a) also indicates that for a given scanning angle, the relative recovered intensity of the deep absorber decreases with the depth. Therefore, it is expected that the deeper absorber would be invisible ($\eta < 0.5$) when it is deep enough relative to the shallow absorber. The above results suggest that there exists a visible depth d_v (relative to the shallow absorber) for a given scanning angle. When the depth is larger than d_v, the deeper absorber could be obscured by the shallower absorber. In other words, to image the absorbers in a given depth, the scanning angle must be larger than a certain angle. Otherwise, the strong shallow image could make the week deep absorber invisible in the image. Figure 5 illustrates the relationship between the visible depth d_v and the scanning angle θ. d_v is defined as the minimum distance between the centers of the absorbers to guarantee $\eta > 0.5$. It can be seen that the visible depth generally increases with the scanning angle. When the scanning angle is 0.28π, the visible depth is only about 6.0 mm.

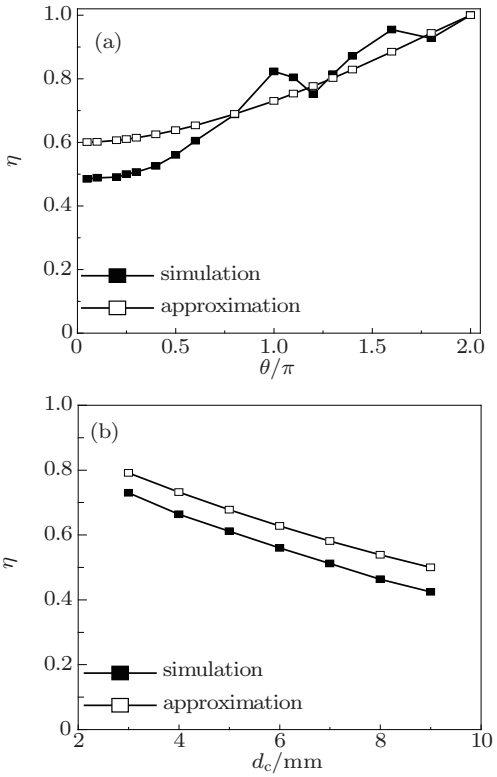


Fig. 4. (a) The maximum reconstructed intensity ratio between the two absorbers with different scanning angles, and an approximation to it with the effective scanning angle method. The distance between the centers of absorbers is $d_c = 6$ mm. (b) The maximum reconstructed intensity ratio between absorbers by altering d_c, and an approximation to it with the effective angle method. The scanning angle is 0.5π.

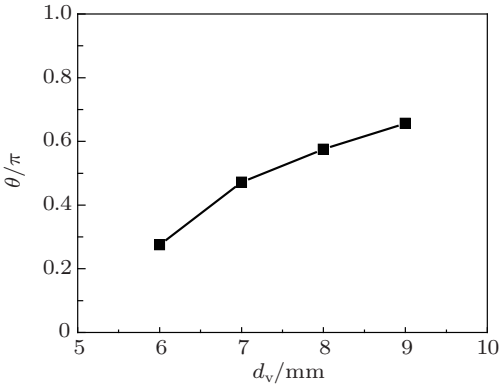


Fig. 5. The relationship between the visible depth d_v and the scanning angle θ.

Finally, a modified reconstruction based on the effective scanning angle is proposed to address the invisibility problem induced by limited-view scanning. It has been shown that the reconstructed intensity ratio of absorbers in different depths can be approximated by their effective scanning angles. Therefore, the intensity difference produced by limited-view scanning can be corrected by multiplying $1/\theta_e$ in Eq. (3), that

is,

$$A(\boldsymbol{r}) \approx -\frac{r_0^2}{2\pi\beta c^4}\int_{\theta_1}^{\theta_2} \mathrm{d}\theta_0 \frac{1}{\theta_\mathrm{e} t}\frac{\partial p\,(\boldsymbol{r}_0, t)}{\partial t}\bigg|_{t=|\boldsymbol{r}-\boldsymbol{r}_0|/c}, \tag{7}$$

where θ_e is the effective scanning angle of reconstructed position, which can be calculated according to Fig. 3. To show the efficiency of the proposed method, the result is provided in Fig. 6. Compared with the result of directly using back-projection method (presented in Fig. 6(a)), the correction with effective scanning angle could strengthen the intensity of the deep absorber and reveal it in image. In particular, in Fig. 6(b), the intensities of the two absorbers are nearly the same, which reflects the actual absorption distribution.

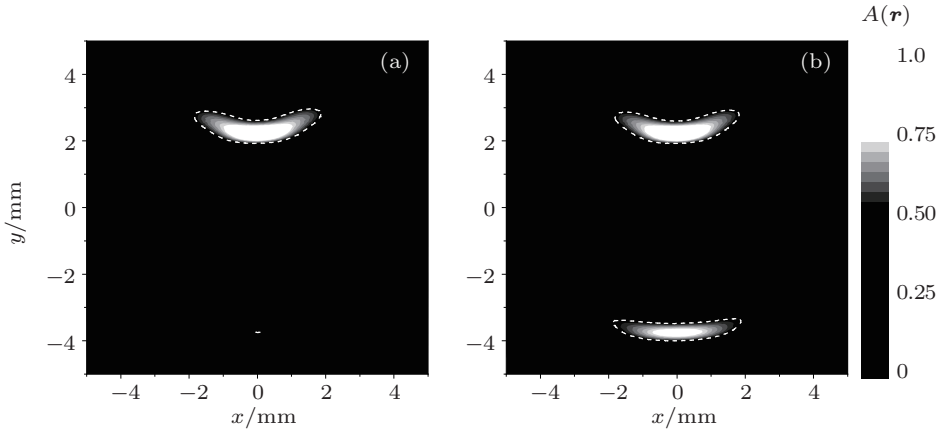


Fig. 6. Comparison between (a) the back-projection method and (b) the proposed method. The dashed lines are the half-maximum contour lines.

4. Conclusion

The influence of limited-view scanning on depth imaging of PAT is quantitatively investigated in this study. When absorbers are located at different depths, incomplete data due to limited-view scanning make the reconstructed intensity of the deep absorber always weaker than that of the shallow one, resulting in the likelihood that the deep absorber will disappear from the reconstructed image. It is likely to induce the invisibility of the deeper absorber in PAT, if the scanning angle is too small. The invisibility of the deep absorber is not due to the attenuation of acoustic signals during propagation, but due to limited-view scanning. The concept of effective scanning angle successfully explains this phenomenon found in our numerical experiments. Finally, we propose a modified reconstruction method, which effectively improves the image quality with limited-view scanning. The quantitative results and the modified method could help devise limited-view scanning trajectory and improve the quality of limited-view reconstruction.

References

[1] Wang L V 2008 *Med. Phys.* **35** 5758
[2] Kong F, Chen Y C, Lloyd H O, Silverman R H, Kim H H, Cannata J M and Shung K K 2009 *Appl. Phys. Lett.* **94** 033902
[3] Cui H Z and Yang X M 2010 *Med. Phys.* **37** 4777
[4] Zhang C, Maslov K and Wang L H V 2010 *Opt. Lett.* **35** 3195
[5] Jansen K, van der Steen A F W, van Beusekom H M M, Oosterhuis J W and van Soest G 2011 *Opt. Lett.* **36** 597
[6] Yao J, Maslov K I, Shi Y, Taber L A and Wang L V 2010 *Opt. Lett.* **35** 1419
[7] Wu D, Tao C and Liu X 2011 *J. Appl. Phys.* **109** 084702
[8] Yuan C Y, Yan Z X, Meng G, Li Z H and Shang L P 2010 *Acta Phys. Sin.* **59** 6908 (in Chinese)
[9] Yang S H and Yin G Z 2009 *Acta Phys. Sin.* **58** 4760 (in Chinese)
[10] Wang X, Pang Y, Ku G, Xie X, Stoica G and Wang L V 2003 *Nat. Biotechnol.* **21** 803
[11] Wang X, Xie X, Ku G, Wang L V and Stoica G 2006 *J. Biomed. Opt.* **11** 024015
[12] Wang X, Chamberland D L and Jamadar D A 2007 *Opt. Lett.* **32** 3002
[13] Wang X, Chamberland D L, Carson P L, Fowlkes J B, Bude R O, Jamadar D A and Roessler B J 2006 *Med. Phys.* **33** 2691
[14] Xiao J Y, Yao L, Sun Y, Sobel E S, He J S and Jiang H B 2010 *Opt. Express* **18** 14359
[15] Xu M and Wang L V 2002 *IEEE Trans. Med. Imag.* **21** 814
[16] Xu M, Xu Y and Wang L V 2003 *IEEE Trans. Biomed. Eng.* **50** 1086
[17] Xu M and Wang L V 2005 *Phys. Rev.* E **71** 016706
[18] Wu D, Tao C and Liu X 2010 *Acta Phys. Sin.* **59** 5845 (in Chinese)
[19] Xu Y, Wang L V, Ambartsoumian G and Kuchment P 2004 *Med. Phys.* **31** 724
[20] Tao C and Liu X 2010 *Opt. Express* **18** 2760
[21] Gamelin J K, Aguirre A and Zhu Q 2011 *Med. Phys.* **38** 1503